Conclusions

The governing equations describing the flowfield that results from the interaction of a centered expansion fan with an oblique shock wave in steady flows were formulated and solved analytically for a perfect inviscid gas.

Since, as mentioned in the Introduction, the interaction of a centered expansion fan with an oblique shock wave is encountered in many steady flowfields, the model developed in the course of this study could assist in investigating these flowfields and improve our understanding of the effect of the various parameters associated with them.

References

[1]Azevedo, D. J., and Liu, S. L., "Engineering Approach to the Prediction of Shock Patterns in Bounded High-Speed Flows," *AIAA Journal*, Vol. 31, 1993, pp. 83–93.

[2]Ben-Dor, G., *Shock Wave Reflection Phenomena*, Springer–Verlag, New York, 1991, Chap. 3.

[3]Ben-Dor, G., "Reconsideration of the State-of-the-Art of the Shock Wave Reflection Phenomenon in the Steady Flows," *JSME International Journal* (to be published).

Automation of Some Operations of a Wind Tunnel Using Artificial Neural Networks

Arthur J. Decker* and Alvin E. Buggele†
NASA Lewis Research Center,
Cleveland, Ohio 44135-3191

Introduction

ARTIFICIAL neural networks have been tested as components for automating wind-tunnel operations in a 3.81 × 10 in. (0.0968 × 0.254 m) subsonic/transonic/supersonic wind tunnel at NASA Lewis Research Center. The authors previously reported an approach to automation[1,2] that uses operator-trained, workstation-resident neural nets as sequencers. Briefly stated, a sequencer estimates for a wind tunnel information such as the next appropriate control settings, flow visualization patterns, or sensor values from the current control settings, flow visualization patterns, or sensor values. The authors intend eventually to have these estimates transmitted, after encoding, to an existing, commercial, programmable logic control system[3] to set the next appropriate state of the tunnel without human intervention. This approach is selected to be minimally intrusive on existing Lewis control systems that accept soft commands. Further discussions and explanations of the theory, the development, and the applications of neural networks, including different uses for control, are left to the extensive literature. A few general references are cited.[4–6]

Artificial neural networks were trained and tested at NASA Lewis Research Center for estimating sensor readings from shadowgraph patterns, shadowgraph patterns from shadowgraph patterns, and sensor readings from sensor readings. This Note will discuss only the results of estimating sensor readings from shadowgraph patterns. Human operators routinely adjust and change, for example, pressure values after viewing flow visualization patterns.

The tunnel was operated with its Mach 2.0 nozzle for this work. Shadowgraph was recorded with a continuous light source and a charge-coupled device (CCD) camera near the nozzle exit. The human operator operated the controls and created the training examples from this mode of flow visualization. The next section discusses the tunnel and its information handling systems.

Operational Procedure and Information Handling

The wind tunnel used to generate the training sets for the neural-net sequencers was actually an upgrade of the first supersonic wind tunnel operated at Lewis Research Center (circa 1946).[7] The highly simplified diagram of Fig. 1 shows the specific components of the tunnel needed to interpret the operational procedure and results. The combustion air valves AC-2408 A and AC-2408 B essentially control the flow. The groups of boundary-layer bleed and exhaust valves were preset for training set generation. In fact, any serious attempt at complete automation would eventually need to recognize that the tunnel uses more than 60 valves.

Flow visualization was acquired through a pair of 47-in. (1.19-m) long windows. The shadowgraph field for this work was actually centered near the right edges of the windows 40 in. (1.02 m) downstream of the nozzle throat or approximately 2 in. (0.05 m) downstream of the nozzle exit. The positional stability and repeatability of the one-pass shadowgraph and the tunnel wall were assured to within 0.002 in. (0.005 cm) using a hard mounted system with taper dowel pins. The actual shadowgraph field recorded was about 10 × 8.5 in. (0.25 × 0.21 m). A sample image is inserted in Fig. 1 for reference.

Figure 1 shows only three of many sensors. The static inlet or plenum pressure is indicated by P_7, and a static test section pressure located 0.5 in. (1.27 cm) downstream of the nozzle exit is indicated by P_8. The Mach number probe MN_3 was located 48 in. (1.22 m) aft of the nozzle throat or about 8 in. (0.2 m) downstream of the

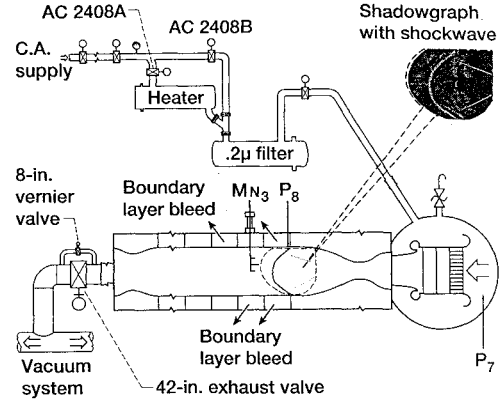

Fig. 1 Tunnel components and shadowgraph field.

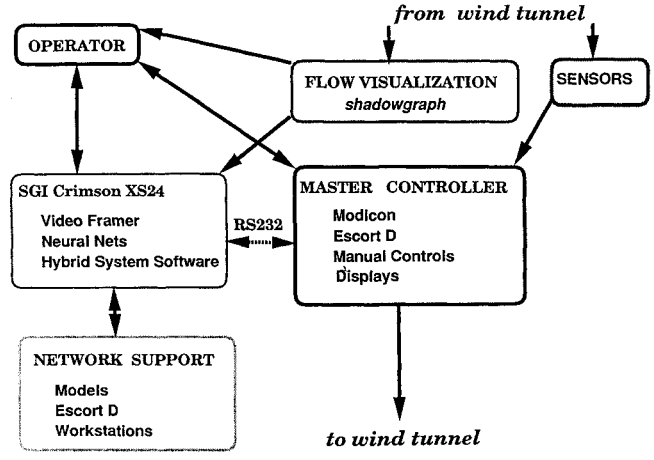

Fig. 2 Flow of information handling and control.

Received April 24, 1995; revision received Sept. 21, 1995; accepted for publication Oct. 9, 1995.

*Senior Research Scientist, Instrumentation and Control Technology Division, 21000 Brookpark Road.

†Senior Operations Engineer, Aeropropulsion Facilities and Experiments Division, 21000 Brookpark Road. Senior Member AIAA.

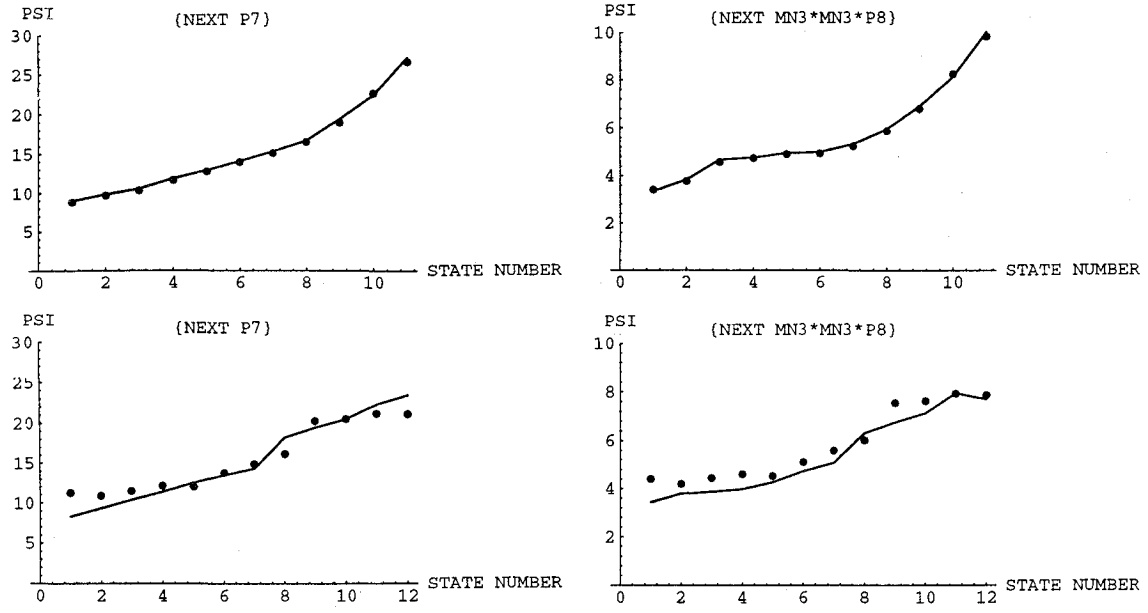

Fig. 3 Performance of shadowgraph-to-sensor sequencer: top row—training; bottom row—test.

nozzle exit. The pressure sensors are, in fact, part of a 186-channel electronically sensed pressure system with an accuracy of ±0.033 psi (±228 Pa). Intrusive upstream and downstream probes and a retention screen induce considerably greater pressure fluctuations [±0.2 psi (1.4 kPa)] than the accuracy implies; the time averages of these fluctuations rather than the accuracy of the transducers determine the tunnel operator's responses and neural-net training sets.

Figure 2 outlines the subsystems used to acquire, handle, and process information on the state of the tunnel as well as exercise control of the wind tunnel. The SGI Crimson XS24 workstation is a key element. All flow visualization patterns enter the computer via a VERSA Module Eurocard mounted, color video frame grabber. A National Television Systems Committee (NTSC) 640 × 480 pixel, black-and-white CCD camera acquires the shadowgraph patterns at 30 frames per second with two fields per frame. Hence unsteady flow visualization patterns are time averaged and may change from one field to the next. At this time, the NASA Lewis ESCORT D central data acquisition system acquires all sensor and control data. These data are transmitted in a few seconds to the workstation's Ethernet connector, via a local area network. Fast acquisition of sensor values and transmission of control information eventually will require direct communications with the tunnel's MODICON programmable logic control system.[3]

A commercial package was used to create the workstation's artificial neural networks.[8] The shadowgraph-to-sensor sequencer discussed in this Note used a three-layer feedforward neural network.[4–6] The lowest layer or input layer contained 3648 inputs to receive 57 × 64 pixel shadowgraph images derived from the 640 × 480 pixel camera images. The second layer, or hidden layer, contained 16 nodes. The third layer, or output layer, contained four nodes to display sensor values. Two of these nodes displayed current sensor values associated with the input shadowgraph pattern. Two of the nodes displayed the next appropriate sensor values in the sequence. The sensor pair selected (Fig. 1) was $[P_7, (MN_3)^2 P_8]$. The combination $(MN_3)^2 P_8$ is less sensitive to variations in the central air handling system and is better correlated with the shadowgraph patterns. This quantity, when divided by P_7, creates a nondimensional ratio that is an approximate invariant. The sequencer required about 3000 iterations per training record for training.

The tunnel operator currently operates the tunnel with manual controls while monitoring the sensor values and flow visualization. Maintaining the integrity of the two one-of-a-kind large optical windows is the major concern during operation of the tunnel for any purpose, including training set generation. Pressure changes are not permitted to exceed 3–6 psi (20–40 kPa) per minute. The major consequence of this requirement is that operations are deliberately performed very slowly. Even the local area network is fast enough for the neural-net experiments. The next section presents the results of training and testing the shadowgraph-to-sensor sequencer.

Results and Discussion

Figure 3 is an example of the results of training shadowgraph-to-sensor sequencers. The figure shows neural-net predictions of the next appropriate sensor values in operations sequences for both training and test sets. The top row of Fig. 3 shows the response of the net to the training set, and the bottom row of Fig. 3 shows the response of the net to the test set. The solid lines in the plots are data-dump sensor values, and the solid dots are net generated sensor values. Each record in the training or test sequence is indexed by an arbitrary tunnel state number.

The runs to record training and test sets were performed about one month apart. Both runs recorded full sensor and visualization data for generating shadowgraph-to-sensor sequences. The training set contains 11 shadowgraph-to-sensor records, and the test set contains 12 records. But the human operator controlled the tunnel from sensors while generating the test set and from shadowgraph only while generating the training set. The training and test records are not identical. The records do not overlap until state 4. Hence, the ability of the net to extrapolate and interpolate is tested.

Concluding Remarks

Figure 3 shows that a tunnel operator can train by example artificial neural networks to estimate the next operating state of a tunnel from a shadowgraph pattern. The human operator is the only judge now whether the estimate is accurate enough to bring the tunnel to a safe, adequate intermediate state and whether the sequence will bring the tunnel to an acceptable final state. The intent is to replace this open-loop testing with a closed-loop test where the neural net sequencer will control the tunnel without human intervention. A software interface to implement this closed-loop control is now being developed by a NASA Lewis Research Center contractor.

References

[1]Decker, A., and Buggele, A., "Wind Tunnel Operations Using Archival Flow Visualization Records and Artificial Neural Networks," AIAA Paper 94-0390, Jan. 1994.

[2]Buggele, A. E., and Decker, A. J., "Control of Wind Tunnel Operations Using Neural Net Interpretation of Flow Visualization Records," NASA TM 106683, Aug. 1994.

[3]MODICON, vended by MODICON AEG, 1 High St., North Andover, MA 01845.

[4]Rumelhart, D. E., McClelland, J. L., and the PDP Research Group, *Parallel Distributed Processing—Explorations in the Microstructure of Cognition, Volume I: Foundations*, MIT Press, Cambridge, MA, 1986.

[5]Pao, Y.-H., *Adaptive Pattern Recognition and Neural Networks*, Addison–Wesley, New York, 1989.
[6]Anon., *Proceedings of the Third Workshop on Neural Networks: Academic/Industrial/NASA/Defense*, Society for Computer Simulation, San Diego, CA, 1992.
[7]Brinich, P. F., "Boundary-Layer Measurements in 3.84- By 10-Inch Supersonic Channel," NACA TN 2203, Oct. 1950.
[8]NeuralWorks Professional II/PLUS, Vended by NeuralWare, Inc., Penn Center West, Building IV, Pittsburgh, PA 15276.

Shape Optimization with Buckling and Stress Constraints

M. E. Botkin*
General Motors Research and Development Center, Warren, Michigan 48090-9055

Introduction

SHAPE optimization of stamped sheet metal parts has been the subject of much research.[1] All of this work has been based on static finite element analysis, which, therefore, permits only the consideration of stress and displacement constraints within the optimization problem. Although several papers exist on optimal sizing variables subject to buckling constraints, only one paper could be found dealing with shape variables.[2] That work addresses the problem of finding the optimal thickness distribution for a rectangular isotropic plate of given plan dimensions (length and width) that would maximize its uniaxial buckling load, loosely referred to as shape optimization. Other similar papers exist on such subjects as the design of stiffeners to maximize the buckling load of plates. The problem to be treated in this paper is the design of the shape of plates or curved shells of arbitrary shape to control the onset of global buckling, defined as follows:

$$[K]\{\phi_n\} + \lambda_n[K_d]\{\phi_n\} = 0$$

in which ϕ_n are the buckling modes, $[K]$ is the global stiffness matrix, $[K_d]$ is the differential stiffness matrix, and λ_n is the buckling load factor. If λ_n is ≤ 1.0, buckling is predicted.

Design variables control the shape of boundaries, holes, and cutouts. Internal mesh points move as the boundaries move using the static displacements of an auxiliary model.[3] A parametric modeling approach is used to define the complete problem, which includes fully automatic mesh generation[4] to create the finite element mesh. A commercial finite element program was used for analysis and sensitivities.[5] A conservative approximate problem formulation[6] is used for optimization in which the approximate problem is solved using the modified method or feasible directions.[7]

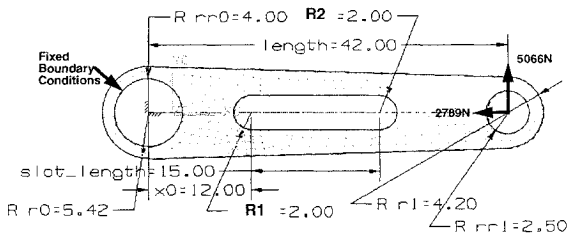

Fig. 1 Parametric torque arm mode (initial design): $E = 60E + 6$ N/cm^2; $\sigma_y = 80{,}000$ N/cm^2; $\rho = 0.00781$ kg/cm^3.

Design Problems

The following problems are designed for minimum mass, i.e., objective function, subject to constraints on the first buckling mode and the maximum effective stress in each element. There is one auxiliary load case per design variable. The analysis uses a four-node (quadrilateral), isoparametric membrane-bending plate element.

Rear Suspension Torque Arm

Analysis Problem

The component shown in Fig. 1 is a rear suspension torque arm, used to prevent windup in live axles. This problem is idealized as fixed around the large hole and loaded, as shown, at the small hole. The part is 0.3 cm thick and assumed to be stamped from sheet metal. For this study, the stresses are assumed to be limited to 80,000 N/cm^2.

Because this is a flat part loaded in the plane, without consideration of buckling, and even though no out-of-plane support exists (except at loading and support points), the only deformations expected would also be in the plane. However, the buckling phenomenon can also occur but is generally ignored. Linear static analysis will not detect buckling, which can be predicted by a separate buckling analysis. For the initial design of the torque arm, the first (lowest) buckling mode can be seen in Fig. 2. This figure shows the highly exaggerated out-of-plane deformation. Buckling occurs first in this

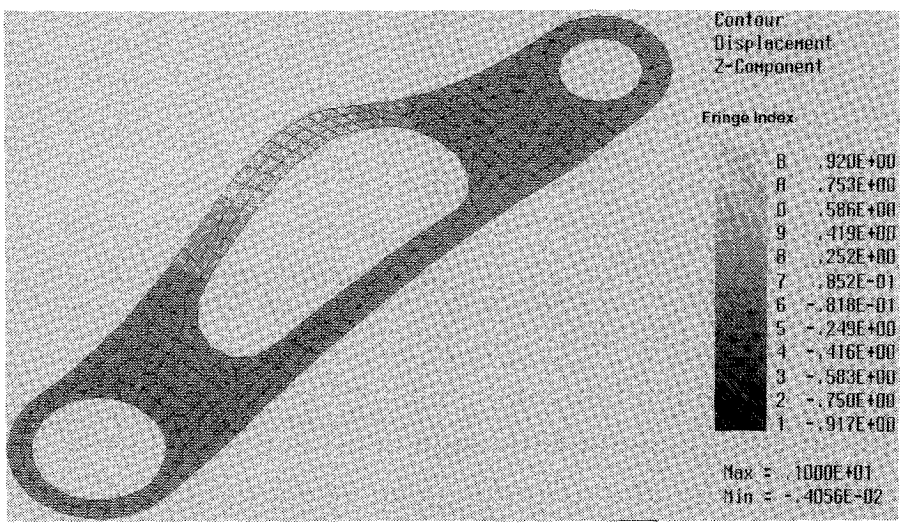

Fig. 2 Buckling mode of torque arm.

Presented as Paper 94-4291 at the AIAA/USAF/NASA/ISSMO 5th Symposium on Multidisciplinary Analysis and Optimization, Panama City Beach, FL, Sept. 7–9, 1994; received June 28, 1995; revision received Oct. 6, 1995; accepted for publication Oct. 9, 1995.

*Principal Reasearch Engineer, Engineering Mechanics Department.